Ultrahigh-Resolution Soft-X-Ray Microscopy with Zone Plates in High Orders of Diffraction

S. Rehbein, S. Heim, P. Guttmann, S. Werner, and G. Schneider

Helmholtz-Zentrum Berlin für Materialien und Energie GmbH, Elektronenspeicherring BESSY II,
Albert-Einstein-Straße 15, 12489 Berlin, Germany

We present an x-ray optical approach to overcome the current limitations in spatial resolution of x-ray microscopes. Our new BESSY full-field x-ray microscope operates with an energy resolution up to $E/\Delta E = 10^4$. We demonstrate that under these conditions it is possible to employ high orders of diffraction for imaging. Using the third order of diffraction of a zone plate objective with 25 nm outermost zone width, 14 nm lines and spaces of a multilayer test structure were clearly resolved. We believe that high-order imaging paves the way towards sub-10-nm real space x-ray imaging.

PACS numbers: 07.85.Tt, 41.50.+h, 07.85.Qe

X-ray imaging techniques offer the unique potential to study thick samples with buried nanoscale structures and provide an element specific image contrast. Many scientific applications in material and life sciences require a spatial resolution in the sub-10-nm range. With conventional zone plate based x-ray microscopy about 25 nm lines and spaces can be resolved. Currently, numerous lensless x-ray imaging approaches are described in the literature to overcome this limitation [1–10]. These approaches showed spatial resolutions better than the resolution of conventional lens based x-ray microscopy with isolated samples [1–3]. With extended relevant samples, lensless coherent diffraction microscopy or holography methods provided so far spatial resolutions in the range of 20–70 nm either at synchrotron or FEL sources [4–7]. However, with lensless imaging methods the difficulty of manufacturing x-ray lenses is shifted towards phase-recovering problems.

Zone plate based microscopy yields directly the image information in real space. In addition, in Zernike phase contrast mode it is possible with the phase ring in the Fourier plane to tune the image contrast of weakly scattering object features to basically any value [11]. The advantage of real space imaging with zone plates stimulated different approaches to overcome the conventional 25 nm (half-pitch) resolution limit. With full-field microscopy, 15 nm lines and spaces were resolved using advanced zone plates with an outermost zone width of 15 nm manufactured by a novel overlay technique [12]. A similar resolution is obtained with scanning microscopes by frequency-doubling of the local zone periods [13].

We report on a different x-ray optical method to significantly improve the resolution for real space imaging with zone plates towards 10 nm. The spatial resolution of an x-ray microscope is limited by the outermost zone width dr_N of the zone plate objective. The traditional way to improve the spatial resolution is the reduction of the zone widths. However, the fabrication of zone plates with zone widths below 15–20 nm is very challenging due to the technological difficulties in the nanofabrication processes.

To overcome the problem to manufacture increasingly smaller zone widths, we employ high orders of diffraction m for imaging. This significantly improves the numerical aperture (NA) of a zone plate objective since $(NA)_m \approx m \times (NA)_1$ scales with the order of diffraction. If the condenser and the objective apertures are matched, third-order imaging already triples the spatial resolution. So far high-order imaging was not successfully employed to overcome the conventional resolution limit of 25 nm half-pitch [14,15].

Zone plates are strongly chromatic lenses. To avoid loss of spatial resolution by chromatic aberrations, the energy resolution should be $E/\Delta E \geq mN$ where N is the number of zones. Until recently, soft x-ray full-field microscopes were only installed at bending magnet beamlines. Their zone plate based linear monochromators provided an energy resolution $E/\Delta E \leq 500$ [16] sufficient for first-order imaging. In contrast, high-order imaging demands an m-fold increased $E/\Delta E$. In addition, as the focal length shrinks linearly with m, the number of zones should be at least $N = 500$ in order to maintain a practical working distance.

The new full-field soft x-ray microscope installed at the undulator beam line U41 at the BESSY II electron storage ring in Berlin overcomes the energy resolution limit of the previous x-ray optical setups by more than 1 order of magnitude [17]. The high energy resolution is obtained by a spherical grating monochromator (SGM). The divergent beam emerging from the exit slit of the monochromator is collected by a single-bounce ellipsoidal glass capillary condenser. The condenser illuminates the object field with a measured focusing efficiency of 80.5% at $E = 0.5$ keV [18]. The capillary generates the required hollow cone illumination while an opaque disk centered in its entrance aperture blocks the direct light (see Fig. 1). With this x-ray optical setup, the image field is free of zero and higher order radiation not used for imaging. The spot size formed by the capillary is only 1 μm × 1 μm [18] and hence too small to illuminate the full field of view.
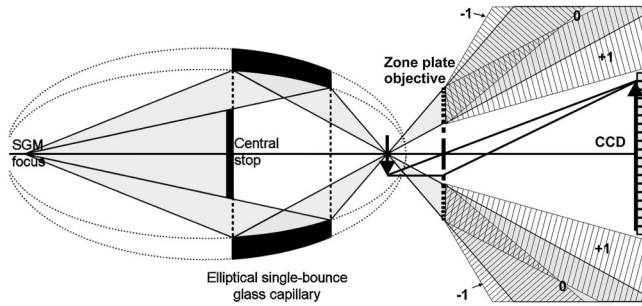
FIG. 1.   X-ray optical setup of the full-field x-ray microscope for third-order imaging. The capillary condenser generates the required hollow cone illumination. The image formed by the third order of diffraction of the zone plate is recorded by the CCD detector. Radiation from other zone plate diffraction orders (as indicated for the zeroth, first and negative first order) forms ring patterns in the image plane due to the hollow cone object illumination.

Therefore, the capillary condenser has to be helically scanned in a plane perpendicular to the optical axis to fully illuminate the object field. The object is imaged with high magnification by the zone plate objective into the image plane and recorded by a two-dimensional 1340×1300 pixel CCD detector. The zone plate objective has an outermost zone width $dr_N = 25$ nm, a diameter of $d = 90$ μm and $N = 900$ zones. The zone material is gold and the zone thickness is $t = 190$ nm. According to electrodynamic theory, the diffraction efficiency of the zone plate is $\eta_1(dr_N = 25\text{nm}) = 13.3\%$ for the first order of diffraction for an x-ray photon energy of $E = 700$ eV [19].

In general, the diffraction efficiency $\eta_m(dr_n, t, E, \tilde{n})$ for the diffraction order m is a function of the local zone width dr_n, the zone thickness t, the photon energy E, the complex index of refraction $\tilde{n}$ as well as the zone profile and line to space ratio of the zones [20–23]. For a spatial resolution of 10 nm, according to the Rayleigh criterion a zone plate objective with an outermost zone width of 8.3 nm would be required in the first order of diffraction. If such a zone plate could be fabricated the maximum efficiency for the non-tilted outermost zones of a classical zone plate would be $\eta_1(dr_N = 8.3\text{ nm}, E = 700\text{ eV}) = 6.1\%$ at a gold zone thickness of $t = 105$ nm [19]. Much higher efficiencies can be obtained for zone plates with tilted zones and high aspect ratios t/dr_n [20–23]. However, so far such zone plates are not existing due to limits of current nanotechnology.

To demonstrate that x-ray imaging in high orders of diffraction is one solution to pave the way towards the 10-nm resolution, we used the above mentioned gold zone plate with $dr_N = 25$ nm in the third order of diffraction. In this case, the diffraction efficiency of the third order of diffraction is of interest. In Fig. 2, the efficiency of the third order of diffraction is plotted as a function of the gold zone thickness and the ratio dr_n/m which scales linearly with the obtainable spatial resolution. The plot shows that the
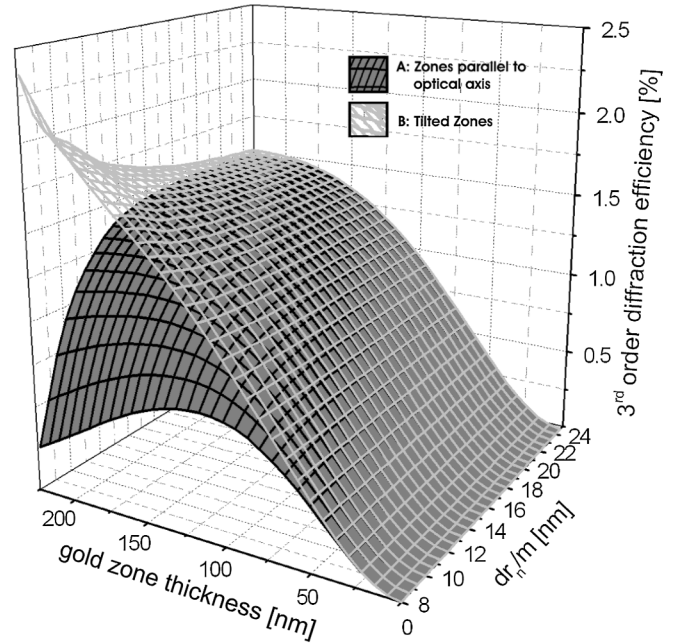

FIG. 2.   Calculated diffraction efficiency $\eta_3(dr_n, E = 700$ eV) of a gold zone plate with line to space ratio 1:1, operating in the order $m = 3$. (a) Calculation for zone structures parallel to the optical axis. (b) Zone structures tilted with respect to the optical axis to fulfil the Bragg condition.

efficiency depends strongly on the zone width. In the described experiment is $dr_N/m = 8.3$ nm resulting in a theoretical efficiency of $\eta_3(dr_N = 25$ nm, $E = 700$ eV$) = 0.57\%$ for the outermost 190 nm thick gold zones (see Fig. 2, plot A for zones parallel to the optical axis). For conventional nontilted zones the maximum third order diffraction efficiency of 0.78% is obtained at a lower zone thickness of 125 nm.

Because of the fabrication process the zone structures of the used objective are parallel to the optical axis of the x-ray microscope. An improvement in the efficiency can be obtained if the zones are tilted to the optical axis to fulfil the local Bragg condition [20–23]. Figure 2 (plot B) shows the calculated third order diffraction efficiency for an optimal local tilt angle of the zones. In the case of appropriately tilted zones, the efficiency of 25 nm wide zones in third order of diffraction ($dr_N/m = 8.3$ nm) is higher and significantly increases with the zone thickness. Electrodynamic theory gives diffraction efficiencies in high orders of up to 30%–50% [19,21]. The realization of such volume zone plates requires additional efforts in nanotechnology.

To measure the achievable spatial resolution with zone plate objectives operated in high orders of diffraction, B_4C/Cr multilayer structures were fabricated with four different periods (half-pitch: 20.6, 17.5, 14.3, 11.0 nm). Focused ion beam (FIB) milling was used to prepare a cross-section of the multilayer structures with about 100 nm thickness. The thin lamella was imaged in the x-ray microscope at $E = 700$ eV photon energy with

$E/\Delta E = 1700$ using the aforementioned zone plate objective in the third order of diffraction. We recorded x-ray images at a 8250-fold magnification on a CCD camera with 20 μm pixel size. This corresponds to a pixel size of 2.4 nm × 2.4 nm in the object plane. In the obtained x-ray microscope images (exposure time 15.7 s), lines and spaces of 20.6, 17.5, and 14.3 nm are clearly resolved while the 11 nm lines and spaces still show some modulation (see Fig. 3). The measured image contrast for the 20 nm lines is about twofold lower than the calculated intrinsic absorption contrast. In the 20 nm region the contrast transfer function (CTF) already decreases the image contrast of the object. Therefore, for quantitative imaging the CTF has to be characterized in more detail.

Until now no sub-20 nm (half-pitch) resolution x-ray images were presented in the literature from extended relevant samples. Besides life science, another application which benefits from ultrahigh spatial resolution imaging is the analysis of electromigration and stress migration in IC technology [24]. To demonstrate the improved resolution in the third order of diffraction for relevant samples, an advanced copper interconnect stack which was thinned by FIB milling to a thin lamella of about 1.5 μm thickness was imaged at $E = 900$ eV. Figures 4(a) and 4(b) show the same object features imaged in the first and third order of diffraction with the same zone plate objective. The x-ray
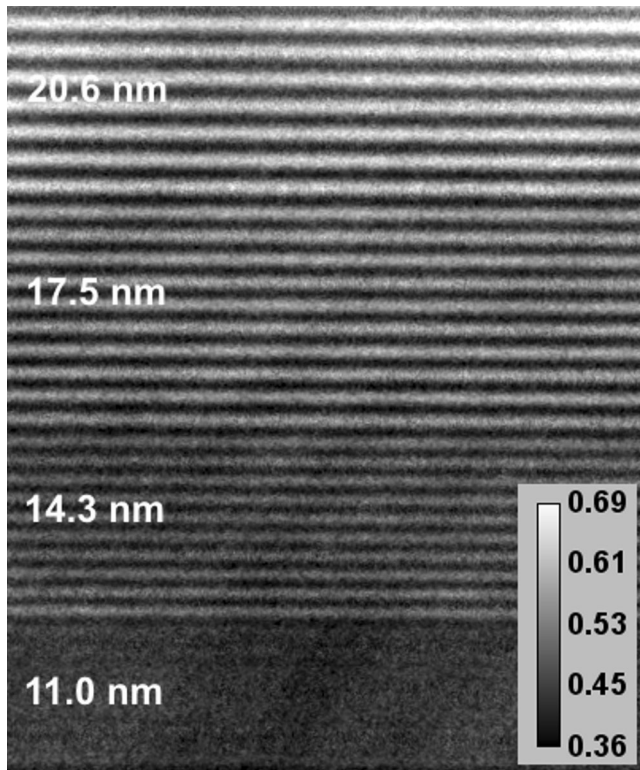
micrographs show the IC stack with the copper interconnect structures embedded in low-k dielectrics. Note that the third-order image reveals the structures in the copper interconnect stack much more clearly as, for example, the sub-10-nm thick barrier layers which prevent the Cu from diffusing into the dielectric material. The images show only a fraction of the obtained x-ray micrographs, the full imaged object field in the third order of diffraction is 4.2 μm × 4.1 μm, each pixel corresponds to 3.1 nm. The depth of field is 200 nm and therefore in the range of the diameter of the via structures. To quantify the resolving power of the microscope, we calculated a power spectrum from the x-ray micrograph of Fig. 4(b) (see Fig. 4 bottom). We find that the cutoff frequency corresponds to a feature size of about 12 nm which is in

FIG. 3. Left: X-ray microscope image of Cr/B$_4$C multilayer structures with 4 different periods recorded in the third order of diffraction. The values of the half pitch of the structures are 20.6, 17.5, 14.3, and 11.0 nm. The image is flat field corrected.
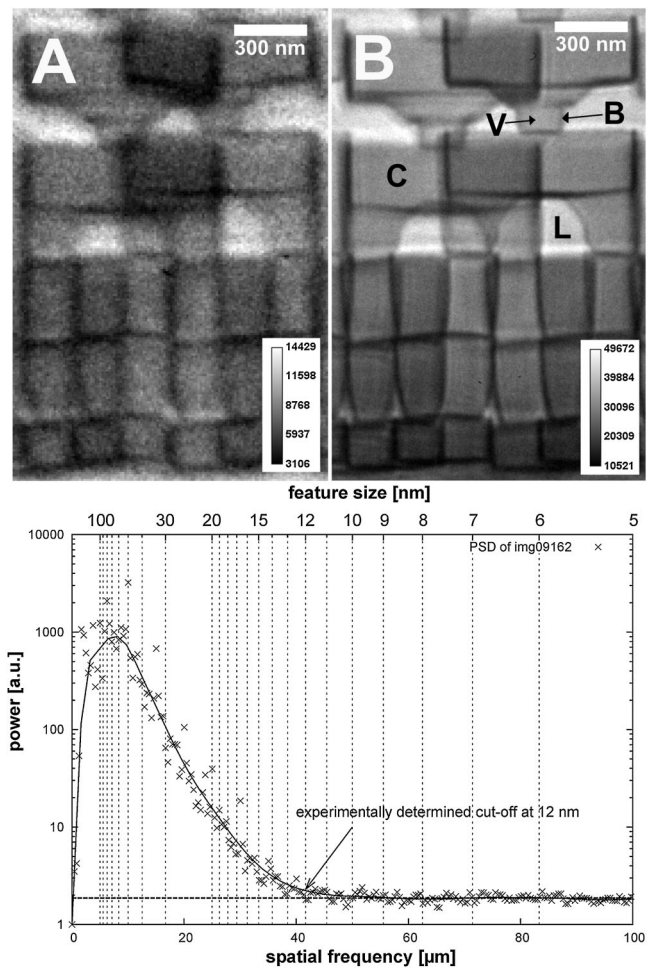

FIG. 4. Top: Sections of x-ray micrographs of an advanced copper interconnect IC stack imaged at 0.9 keV photon energy. Image A was obtained in the first order of diffraction with an energy resolution of $E/\Delta E = 4300$ and an exposure time of 5.2 s. Image B was obtained in third order of diffraction, energy resolution $E/\Delta E = 1400$, exposure time 26 s. Abbreviations: V = via, B = barrier layer, C = interconnect structure, L = low-k dielectrics. Bottom: Power spectrum of image B. The cutoff frequency corresponds to 12 nm feature size.

good agreement with the obtained resolution demonstrated with the multilayer structures.

The presented results show that full-field x-ray microscopy is closely approaching the 10 nm spatial resolution. In fact, with the described x-ray optical setup the theoretical cutoff frequency for the zone plate employed in the third order of diffraction and the used condenser corresponds to 7 nm feature size. The discrepancy to the measured cutoff value of 12 nm is mainly due to remaining zone positioning errors [25]. Originally, the zone plate was designed for the first order of diffraction for imaging at $E = 516$ eV photon energy whereas the measurements were performed by employing the third order of diffraction at $E = 700$ and 900 eV. The deviation of the local zone positions from the ideal design geometry causes spherical aberrations. However, spherical aberrations can be avoided by fabricating zone plates designed for the specific imaging geometry for the third order of diffraction using a high precision e-beam writer. Furthermore, electrodynamic theory of the diffraction efficiency gives that the zone structures have to be tilted with respect to the optical axis to fulfil the local Bragg condition for an optimal performance. Violating the Bragg condition not only reduces the diffraction efficiency but also introduces aberrations which degrade the spatial resolution. To overcome this problem, either low efficient zone plates with nontilted, low aspect ratio zones or high efficient volume zone plates with tilted, high aspect ratio structures have to be employed.

The advantage of high-order imaging is the significantly improved spatial resolution compared to the conventional first-order imaging mode. The disadvantage is the low efficiency of current zone plates used in high orders of diffraction which causes an increased radiation dose deposited in the object in full-field x-ray microscopy. However, volume zone plates optimized for high orders can solve this problem by combining high resolving power and high diffraction efficiency exceeding the current efficiency values for third-order imaging by more than an order of magnitude [19,21–23].

In summary, our results demonstrate the possibility to apply higher orders of diffraction of a zone plate objective to significantly improve the spatial resolution in full-field x-ray imaging. By using a zone plate with 25 nm outermost zone width in the third order of diffraction a spatial resolution of 14.3 nm is achieved. Furthermore, we showed that the exposure time is still very short for high resolution x-ray imaging. In the future, volume zone plates optimized for high-order imaging have the potential to reduce the dose applied to the sample by more than an order of magnitude and push the spatial resolution of state of the art x-ray microscopes to sub-10-nm.

[1] C. G. Schroer *et al.*, Phys. Rev. Lett. **101**, 090801 (2008)
[2] A. Barty *et al.*, Phys. Rev. Lett. **101**, 055501 (2008).
[3] H. Jiang *et al.*, Phys. Rev. Lett. **100**, 038103 (2008).
[4] B. Abbey *et al.*, Appl. Phys. Lett. **93**, 214101 (2008).
[5] D. Shapiro *et al.*, Proc. Natl. Acad. Sci. U.S.A. **102**, 15 343 (2005).
[6] S. Eisebitt *et al.*, Nature (London) **432**, 885 (2004).
[7] P. Thibault, M. Dierolf, A. Menzel, O. Bunk, C. David, and F. Pfeiffer, Science **321**, 379 (2008).
[8] J. M. Rodenburg *et al.*, Phys. Rev. Lett. **98**, 034801 (2007).
[9] H. N. Chapman *et al.*, Nature Phys. **2**, 839 (2006).
[10] L.-M. Stadler *et al.*, Phys. Rev. Lett. **100**, 245503 (2008).
[11] G. Schneider, Ultramicroscopy **75**, 85 (1998).
[12] W. Chao, B. D. Harteneck, J. A. Liddle, E. H. Anderson, and D. T. Attwood, Nature (London) **435**, 1210 (2005).
[13] K. Jefimovs, J. Vila-Comamala, T. Pilvi, J. Raabe, M. Ritala, and C. David, Phys. Rev. Lett. **99**, 264801 (2007).
[14] G.-C. Yin *et al.*, Appl. Phys. Lett. **89**, 221122 (2006).
[15] G. Schmahl, D. Rudolph, and B. Niemann, J. Phys. (Paris), Colloq. **39**, C4-202 (1978).
[16] B. Niemann, D. Rudolph, and G. Schmahl, Opt. Commun. **12**, 160 (1974).
[17] G. Schneider, P. Guttmann, S. Heim, S. Rehbein, D. Eichert, and B. Niemann, AIP Conf. Proc. **879**, 1291 (2007).
[18] P. Guttmann, X. Zheng, M. Feser, S. Heim, W. Yun, and G. Schneider, Proceedings of the 9th International Conference on X-Ray Microscopy, Zürich, Switzerland, 2008, (to be published).
[19] See EPAPS Document No. E-PRLTAO-103-045939 for calculations of the diffraction efficiency in the order $m = 1$ and $m = 3$. For more information on EPAPS, see http://www.aip.org/pubservs/epaps.html.
[20] J. Maser and G. Schmahl, Opt. Commun. **89**, 355 (1992).
[21] G. Schneider, Appl. Phys. Lett. **71**, 2242 (1997).
[22] S. Rehbein and G. Schneider, *Proceedings of the 8th International Conference on X-ray Microscopy*, edited by S. Aoki, Y. Kagoshima, and Y. Suzuki, IPAP Conf. Series (The Institute of Pure and Applied Physics, Tokyo, 2006), Vol. 7, p. 103.
[23] G. Schneider, S. Rehbein, and S. Werner, in: *Modern Developments in X-Ray and Neutron Optics*, edited by A. Erko, M. Idir, T. Krist, and A. G. Michette (Springer Berlin, Heidelberg, 2008), p. 137.
[24] G. Schneider *et al.*, AIP Conf. Proc. **817**, 217 (2006).
[25] Y. Vladimirsky and H. W. P. Koops, J. Vac. Sci. Technol. B **6**, 2142 (1988).